nature biomedical engineering

ARTICLES

https://doi.org/10.1038/s41551-021-00749-2

Check for updates

# Generation of systemic antitumour immunity via the in situ modulation of the gut microbiome by an orally administered inulin gel

Kai Han[1,2], Jutaek Nam[1,2], Jin Xu[1,2], Xiaoqi Sun[1,2], Xuehui Huang[1,2], Olamide Animasahun[2,3,4], Abhinav Achreja[2,3,4], Jin Heon Jeon[2,3,4], Benjamin Pursley[5], Nobuhiko Kamada[6], Grace Y. Chen[5], Deepak Nagrath[2,3,4,7] and James J. Moon[1,2,3,7] ✉

**The performance of immune-checkpoint inhibitors, which benefit only a subset of patients and can cause serious immune-related adverse events, underscores the need for strategies that induce T-cell immunity with minimal toxicity. The gut microbiota has been implicated in the outcomes of patients following cancer immunotherapy, yet manipulating the gut microbiome to achieve systemic antitumour immunity is challenging. Here we show in multiple murine tumour models that inulin—a widely consumed dietary fibre—formulated as a 'colon-retentive' orally administered gel can effectively modulate the gut microbiome in situ, induce systemic memory-T-cell responses and amplify the antitumour activity of the checkpoint inhibitor anti-programmed cell death protein-1 (α-PD-1). Orally delivered inulin-gel treatments increased the relative abundances of key commensal microorganisms and their short-chain-fatty-acid metabolites, and led to enhanced recall responses for interferon-γ$^+$CD8$^+$ T cells as well as to the establishment of stem-like T-cell factor-1$^+$PD-1$^+$CD8$^+$ T cells within the tumour microenvironment. Gels for the in situ modulation of the gut microbiome may be applicable more broadly to treat pathologies associated with a dysregulated gut microbiome.**

Although immune-checkpoint blockers (ICB) have drastically changed the landscape of cancer therapy, only a small subset of patients respond to ICB therapy[1,2]. Recent studies have highlighted the vast potential of targeting the gut microbiome for the treatment of inflammatory, metabolic and neurodegenerative diseases as well as cancer[3–6]. In particular, dysregulated gut microbiota has been implicated in the lack of response to ICB therapy[7–13], and clinical investigations are underway to restore healthy gut microbiota in patients with cancer either by inoculation of pre-defined probiotics or faecal microbiota transplantation (FMT). However, a favourable consortium of probiotics for cancer therapy remains ill-defined, and the scale-up manufacturing and quality control of FMT products are challenging. In fact, the Food and Drug Administration (FDA) has recently issued an urgent safety warning on FMT procedures due to fatalities resulting from inadvertent transfers of antibiotic-resistant microorganisms from a donor to recipients[14]. Microbiome-derived metabolites, including short-chain fatty acids (SCFAs), may serve as the key messengers between the gut microbiota and the immune system of the host[15] but it remains unclear how microbial metabolites impact T-cell immunity and how to exploit this knowledge for cancer therapy. Here we report a dietary fibre-based engineering strategy for in situ modulation of the gut microbiome as a safe and straightforward approach for amplifying the systemic memory-T-cell responses and potentiating the therapeutic efficacy of ICB.

Briefly, we screened the FDA's list of ingredients generally recognized as safe (GRAS) and found that oral administration of inulin, a polysaccharide dietary fibre found in chicory root and Jerusalem artichoke, improved the antitumour efficacy of anti-programmed cell death protein-1 (α-PD-1) ICB therapy. Because 'beneficial' commensal microorganisms (for example, *Akkermansia*, *Lactobacillus* and *Roseburia*) that are prevalent in ICB-responsive patients primarily reside in the colon[9–11], we engineered 'colon-retentive' inulin by formulating it into an oral gel. Oral administration of the inulin gel effectively modulated the gut microbiota in situ and promoted the proliferation of commensal microorganisms with beneficial roles in T-cell immunity. This triggered microbial metabolite-mediated differentiation of CD8$^+$ T cells into stem-like memory CD8$^+$ T cells that synergized with α-PD-1 therapy (Fig. 1). Given the long history of inulin as a food ingredient with excellent safety profiles and the facile production process for inulin gel, our approach may open new opportunities for improving the antitumour effects of ICB.

## Results

**Inulin improves the efficacy of α-PD-1 therapy.** We chose candidates from the FDA GRAS list that are known to modulate the gut microbiome and examined whether they could improve the therapeutic efficacy of α-PD-1 ICB. (−)-Epigallocatechin gallate (EGCG), a natural antioxidant found in green tea and red wine, has been shown to alter the gut microbiome[16], whereas fucoidan, fructooligosaccharides (FOS) and inulin are dietary fibres known to increase the richness and diversity of the gut microbiota[17]. We also examined melatonin, which regulates the sleep cycle and circadian rhythm as well as the gut microbiome[18]. We first examined these

[1]Department of Pharmaceutical Sciences, University of Michigan, Ann Arbor, MI, USA. [2]Biointerfaces Institute, University of Michigan, Ann Arbor, MI, USA. [3]Department of Biomedical Engineering, University of Michigan, Ann Arbor, MI, USA. [4]Department of Chemical Engineering, University of Michigan, Ann Arbor, MI, USA. [5]Division of Hematology and Oncology, Department of Internal Medicine, University of Michigan, Ann Arbor, MI, USA. [6]Division of Gastroenterology, Department of Internal Medicine, University of Michigan, Ann Arbor, MI, USA. [7]Rogel Cancer Center, University of Michigan, Ann Arbor, MI, USA. ✉e-mail: moonjj@umich.edu

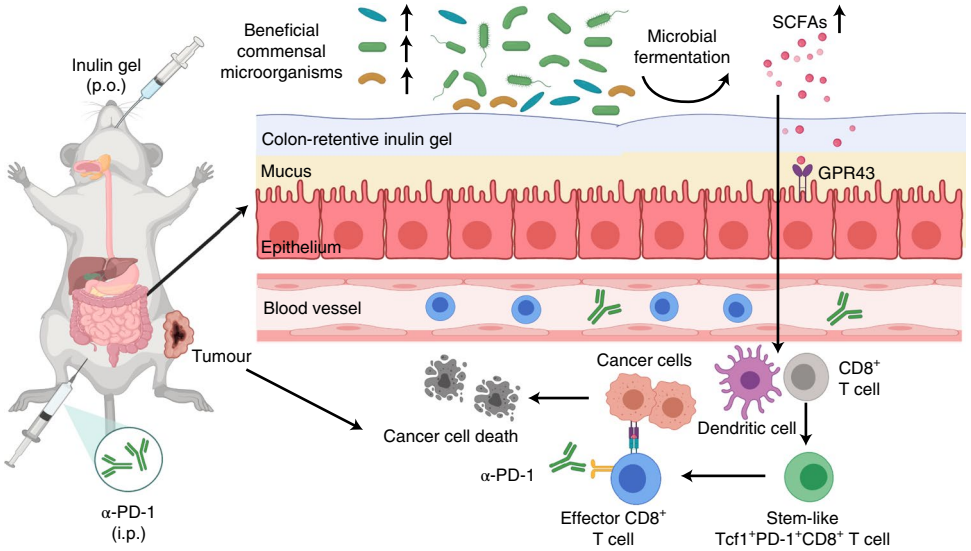


**Fig. 1 | In situ modulation of the gut microbiome with colon-retentive inulin gel for improving cancer immunotherapy.** Orally administered (p.o.) inulin gel increases the levels of beneficial commensal microorganisms and their metabolites, including SCFAs that induce stem-like Tcf1$^+$PD-1$^+$CD8$^+$ T cells. Inulin gel synergizes with α-PD-1 IgG immunotherapy, exerting potent antitumour efficacy in multiple tumour models.

agents in a prophylactic setting. BALB/c mice were pretreated with these agents via oral gavage for one week and then subcutaneously (s.c.) inoculated in their flank with CT26 colon carcinoma cells on day 0 (Fig. 2a). On days 10, 14, 18 and 22, the animals were co-treated by systemic intraperitoneal (i.p.) administration of α-PD-1 IgG. The mice were kept on normal mouse chow diet throughout the study and all treatments were stopped on day 26. Interestingly, oral gavage with inulin significantly improved the systemic antitumour efficacy of α-PD-1 treatment and effectively slowed the growth of CT26 tumours located near the site of the s.c. injection (Fig. 2b,c). In fact, 60% of the mice in the inulin plus α-PD-1 treatment group remained tumour-free throughout the study (Fig. 2b–d), compared with 20% tumour-free mice in the α-PD-1 monotherapy group. Oral gavage with fucoidan also moderately improved the efficacy of α-PD-1 treatment. Inulin, as well as other agents, did not significantly alter the body weight of mice (Supplementary Fig. 1). Compared with α-PD-1 alone, inulin plus α-PD-1 substantially increased the frequency of the circulating CD8$^+$ T cells specific to an immunodominant epitope from CT26 gp70 (AH1, H-2L$^d$-restricted SPSYVYHQF; Fig. 2e and Supplementary Fig. 2a).

We next evaluated these combination therapies in a therapeutic setting in tumour-bearing mice. BALB/c mice were s.c. inoculated with CT26 cells in their flank on day 0 and the treatments were initiated on day 7 (Fig. 2f). Similar to the previous results, inulin plus α-PD-1 significantly slowed tumour growth (Fig. 2g,h) and increased the survival rate compared with α-PD-1 alone (Fig. 2i). Inulin plus α-PD-1 induced a 2.2-fold higher frequency of AH1-specific CD8$^+$ T cells among the peripheral blood mononuclear cells (PBMCs) compared with α-PD-1 alone (Fig. 2j and Supplementary Fig. 2b). Notably, oral administration of inulin alone resulted in a comparable antitumour effect and AH1-specific CD8$^+$ T-cell response to α-PD-1 IgG monotherapy (Supplementary Fig. 3), showing the crucial combination effects of inulin plus α-PD-1 therapy.

**Inulin alters the gut microbiome.** We next examined changes in the gut microbiome by analysing the mouse faecal samples through 16S ribosomal RNA gene sequencing. Although all of the treatment groups exhibited similar richness and diversity of the gut microbiota from the operational taxonomic unit (OTU) and inverse Simpson diversity values (Supplementary Fig. 4), α-PD-1 therapy combined with inulin, FOS or fucoidan induced distinct clustering of the microbial community structure, as shown by the non-metric multidimensional scaling analysis (NMDS, known as β-diversity; Fig. 3a). Specifically, compared with α-PD-1 monotherapy, treatment with inulin plus α-PD-1 significantly increased the relative abundances of some bacterial genera—that is, *Akkermansia*, *Lactobacillus* and *Roseburia* (Fig. 3b–d)—that have been clinically associated with ICB-responsive patients[7–9,11]. In particular, α-PD-1 treatment alone caused the depletion of *Roseburia*, which was normalized with inulin co-treatment (Fig. 3d). *Lactobacillus* and *Roseburia* are known as the major producers of SCFAs such as acetate, propionate and butyrate[19–21], and accordingly, treatment with inulin plus α-PD-1 increased the levels of SCFAs and lowered the pH of the faecal samples in comparison to α-PD-1 monotherapy (Fig. 3e and Supplementary Fig. 5). Spearman's correlation coefficient analyses suggested that the tumour sizes were inversely correlated to the relative abundances of *Akkermansia* and *Lactobacillus* (Fig. 3f), and there was also a trend for an inverse correlation between the tumour size and the levels of *Roseburia*, propionate and butyrate (Supplementary Fig. 6). These results suggest a potential link between the commensal microorganisms, their SCFA metabolites and the treatment outcomes of ICB therapy. Based on the potent modulation effect of the gut microbiome, antitumour effects and the antitumour CD8$^+$ T-cell response, we focused on improving the inulin plus α-PD-1 combination therapy for the remainder of the study.

**Oral inulin gel for improved modulation of the gut microbiome.** As these commensal microorganisms primarily reside in the colon, we examined whether the impact of inulin on antitumour responses could be further improved using inulin formed into an oral hydrogel with colon-retentive properties. This was motivated by previous studies showing that polysaccharide fibres in a gel state can prolong gastric emptying (due to thickening effect), adsorb to the intestinal mucous layer and prolong the residence time[22]. To test this idea, we have developed an oral inulin-gel formulation with a meso-fibrous morphology via a simple heating–cooling method, which is amenable to large-scale production (Fig. 4a–c and Supplementary Fig. 7). We employed a dose of 60 mg inulin in all of the subsequent studies, presenting a 50% reduction from the

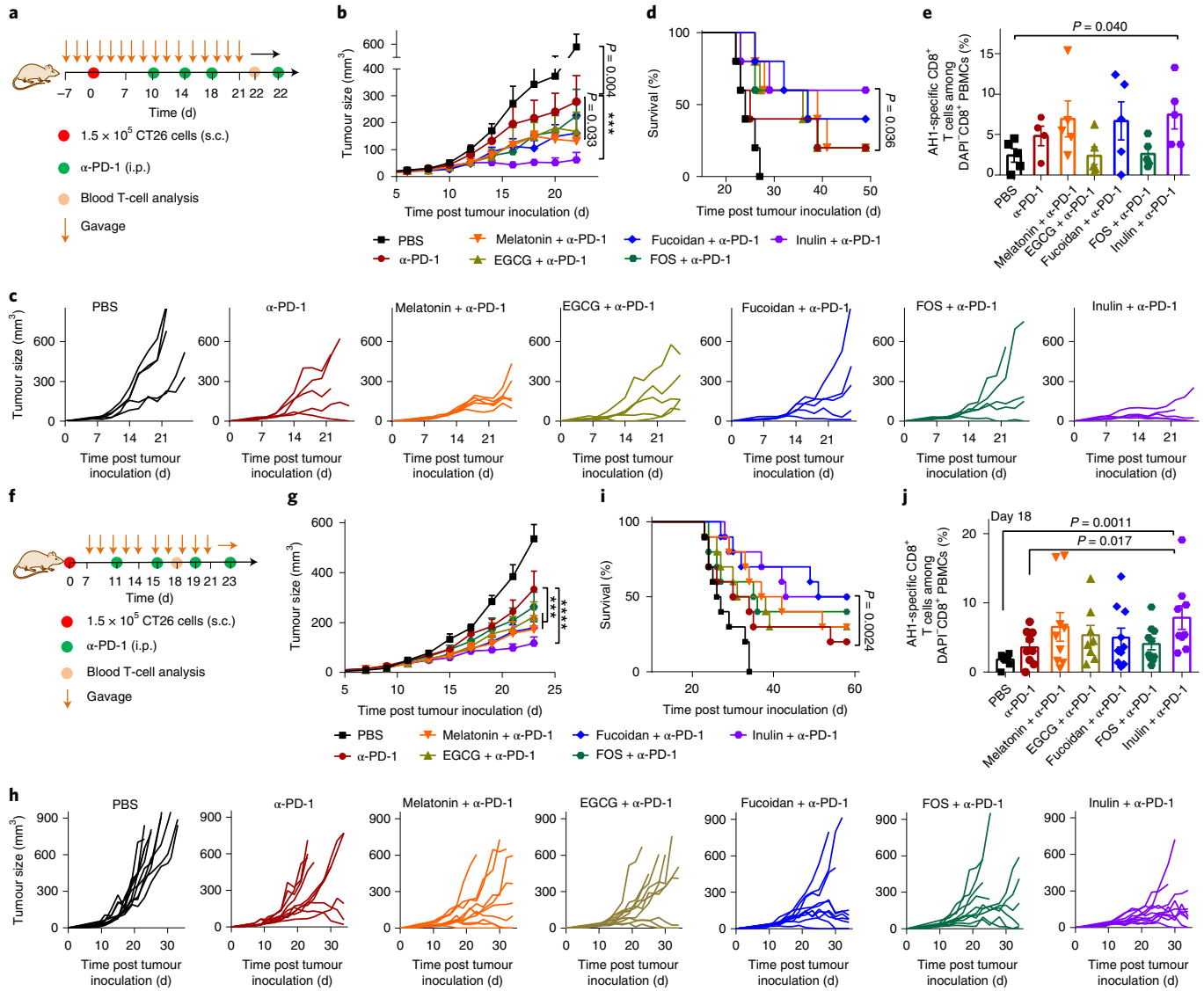


**Fig. 2 | Improving the antitumour efficacy of α-PD-1 therapy with oral candidate agents. a**, Prophylactic treatment regimen. BALB/c mice kept on a normal chow diet were orally gavaged with the candidate agents (melatonin and EGCG, 100 mg kg$^{-1}$ body weight; fucoidan, 200 mg kg$^{-1}$ body weight; and FOS and inulin, 120 mg per dose) starting one week before s.c. inoculation with $1.5 \times 10^5$ CT26 colon carcinoma cells. The mice received the candidate agents until day 26, and 100 μg α-PD-1 was injected i.p. on days 10, 14, 18 and 22. **b**–**e**, Average tumour growth (**b**), individual tumour growth (**c**) and overall Kaplan–Meier survival (**d**) curves as well as the frequency of AH1-specific CD8$^+$ T cells in the peripheral blood on day 22 (**e**) for **a**. **f**, Therapeutic treatment regimen. BALB/c mice were s.c. inoculated in the flank with $1.5 \times 10^5$ CT26 cells and then treated as shown starting on day 7. The doses were the same as in **a**. **g**–**j**, Average tumour growth (**g**), individual tumour growth (**h**) and overall Kaplan–Meier survival (**i**) curves as well as the frequency of AH1-specific CD8$^+$ T cells on day 18 (**j**) for **f**. Data represent the mean ± s.e.m. from a representative experiment ($n = 5$ (**a**–**e**) and 9 or 10 (**f**–**j**) biologically independent samples) of two independent experiments. ***$P < 0.001$, ****$P < 0.0001$. Data were analysed using a two-way ANOVA (**b**,**g**) or one-way ANOVA with Bonferroni's multiple comparisons test (**e**,**j**), or a log-rank Mantel–Cox test (**d**,**i**).

studies shown earlier. Compared with fluorescein isothiocyanate (FITC)–inulin, oral gavage with FITC-labelled inulin gel indicated that the inulin gel was retained longer in the colon (and caecum) in a gel strength-dependent manner (Fig. 4d,e and Supplementary Fig. 8), thereby increasing the cumulative inulin exposure in the colon (Fig. 4f). To examine the impact of inulin gel on the microbial community structure of the gut, mice were inoculated with CT26 cells on day 0 and treated with oral gavage of inulin or inulin gel starting on day 7, followed by α-PD-1 treatment on days 10, 14 and 18 (Fig. 4g). Inulin gel with prolonged colon retention further induced a distinct shift in the microbial community structure of the gut by day 21 in comparison to inulin (Fig. 4h and Supplementary Fig. 9a,b). In particular, compared with free inulin plus α-PD-1, treatment with inulin gel plus α-PD-1 further increased the relative abundances of *Akkermansia* (Fig. 4i,j) and there was a trend for an increased abundance of *Roseburia*, although this was not statistically significant. Notably, lipopolysaccharide-producing *Oscillibacter* was significantly reduced in mice treated with either inulin or inulin gel combined with α-PD-1 (Supplementary Fig. 9c).

**Potent antitumour efficacy of oral inulin gel plus α-PD-1 therapy.** Having shown the impact of inulin gel on the gut microbiome, we sought to assess the antitumour efficacy of the inulin gel plus α-PD-1 therapy. Compared with free inulin plus α-PD-1, the inulin gel plus α-PD-1 combination therapy markedly delayed tumour growth and increased the rate of complete tumour regression by

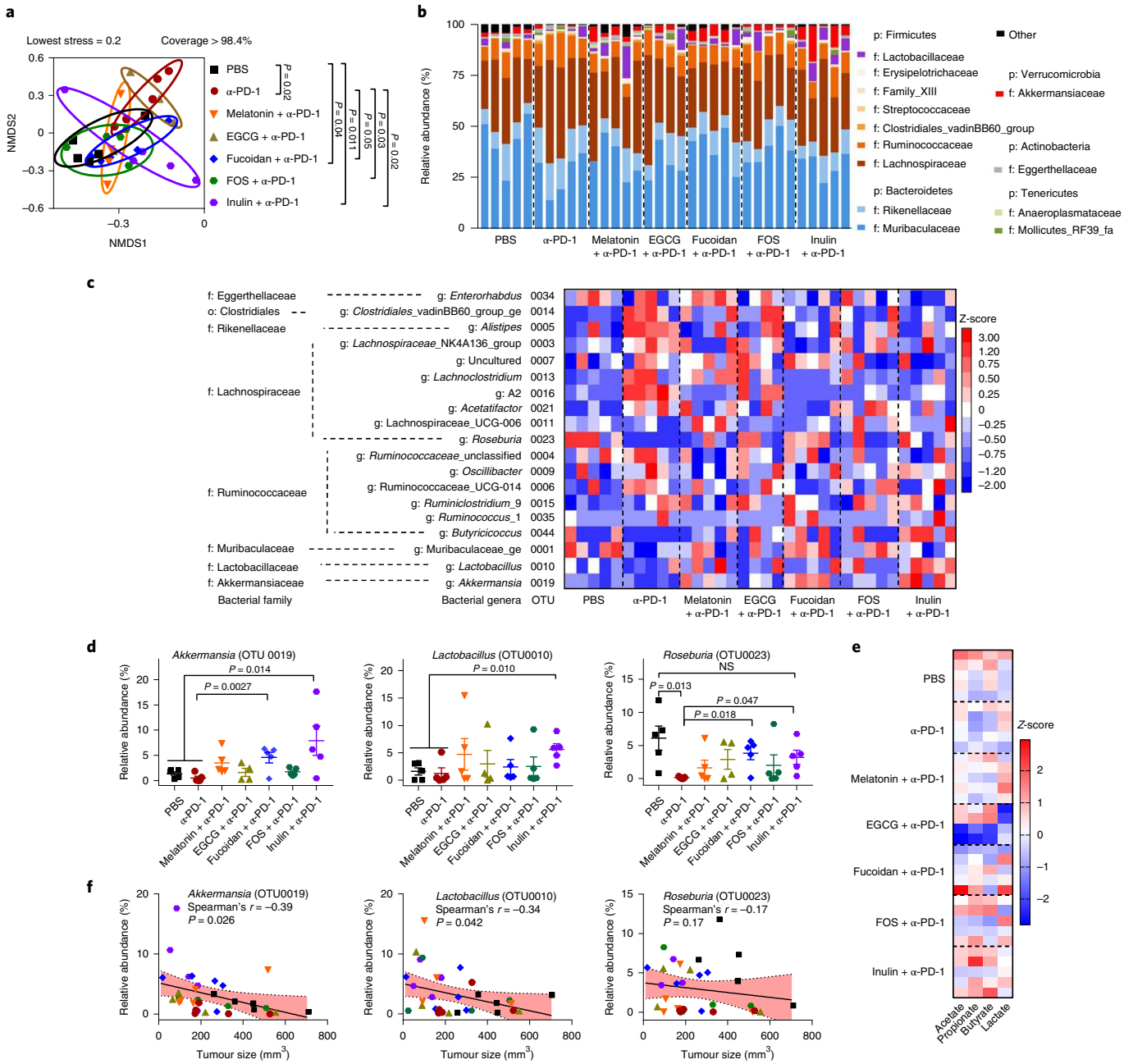


**Fig. 3 | Distinct gut microbial communities promoted by treatment with inulin plus α-PD-1.** CT26 tumour-bearing BALB/c mice were treated as in Fig. 2f and faecal pellets collected on day 21 were analysed using 16S rRNA gene sequencing. **a**–**e**, NMDS score plot (based on Bray–Curtis; **a**); relative abundances of the gut commensal microorganisms at the phylum and family levels (**b**); heatmap showing the normalized *Z*-score values of microorganism abundances at the family and genus levels (**c**); relative abundances of *Akkermansia*, *Lactobacillus* and *Roseburia* (**d**); and heatmap showing the normalized *Z*-score values of acetate, propionate, butyrate and lactate in the faecal pellets (**e**). **b**,**c**, p, phylum; o, order; f, family; g, genus. NS, not significant. **f**, Spearman's correlation between tumour size and the relative abundance of *Akkermansia*, *Lactobacillus* and *Roseburia*. The shaded band indicates the 95% confidence interval of the values fitted by linear regression. Data represent the mean ± s.e.m. from a representative experiment ($n = 5$ biologically independent samples) of two independent experiments. Data were analysed using an analysis of molecular variance (**a**), one-way ANOVA with Bonferroni's multiple comparisons (**d**) or Spearman's rank correlation (**f**) test.

twofold (Fig. 5a–d). The antitumour efficacy of the combination therapy was dependent on the dose of inulin gel (Supplementary Fig. 10). On the other hand, oral administration of inulin gel alone exhibited only a modest antitumour effect similar to α-PD-1 IgG monotherapy (Supplementary Fig. 11), showing the importance of the inulin gel plus α-PD-1 combination therapy. Interestingly, compared with α-PD-1 given with or without free inulin, inulin gel plus α-PD-1 augmented the systemic antitumour $CD8^+$ T-cell responses, as evidenced by significantly higher frequencies of AH1-specific $CD8^+$ T cells among PBMCs and interferon (IFN)-$\gamma^+CD8^+$ T cells in the spleen (Fig. 5e,f and Supplementary Fig. 12). In addition, inulin gel plus α-PD-1 increased the frequencies of intratumoral $CD8^+$, AH1-tetramer$^+CD8^+$ and $CD4^+$ T cells, activated $CD86^+CD11c^+$ dendritic cells and resulted in a decrease in PD-$1^+CD8^+$ T cells (Fig. 5g,h). Moreover, the surviving mice in the inulin gel plus α-PD-1 group were completely protected against

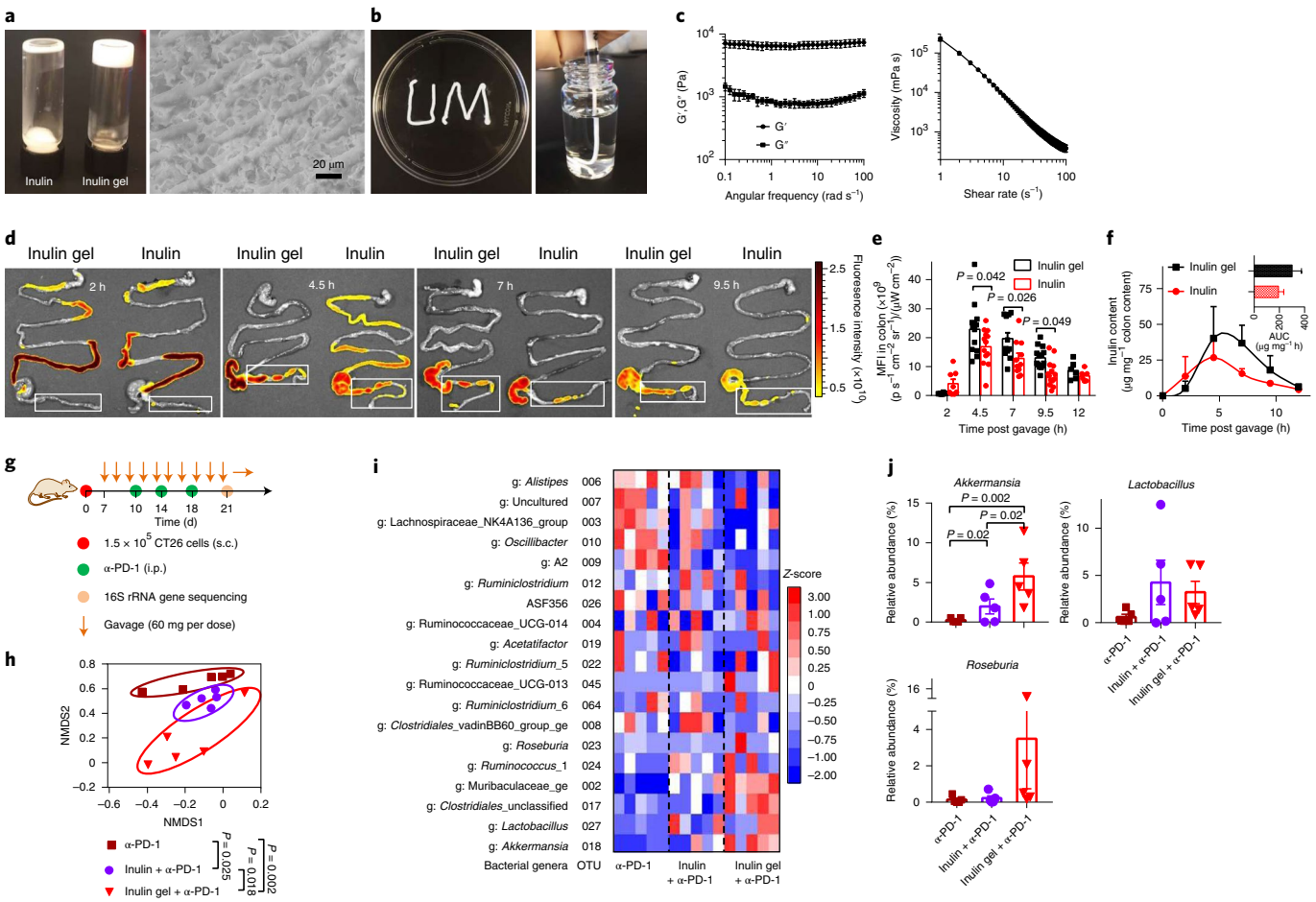


**Fig. 4 | Colon-retentive inulin gel for the modulation of the microbial communities of the gut. a**,**b**, Images of inulin gel for colon-targeting after oral administration. **a**, Digital photo (left) and scanning electron microscopy image (right) of inulin gel. **b**, Photos show injectable inulin gels. **c**, Dynamic rheological testing of inulin gel; G′ (elastic modulus) and G′′ (viscous modulus) (left), and viscosity (right) measurements of inulin gel. **d**,**e**, Mice were orally gavaged with FITC-labelled inulin gel or inulin (60 mg per dose), followed by visualization of the gastrointestinal tract over 12 h (**d**) and measurement of the mean fluorescence intensity (MFI; **e**) in the colon. **d**, Representative images from three biologically independent samples in each group are shown. White box, colon tissue. **f**, The inulin content in colon digesta was quantified using unlabelled inulin or inulin gel. Inset: values for the area under the curve (AUC). **g**–**j**, CT26 tumour-bearing BALB/c mice were treated with inulin or inulin gel starting on day 7, followed by α-PD-1 treatment as indicated. **g**, Treatment regimen. **h**–**j**, The faecal samples from **g** were analysed on day 21 via 16S rRNA gene sequencing. NMDS score plot (**h**), heatmap showing the normalized *Z*-score values of the microorganism abundance at genus level (g; **i**) and relative abundances of *Akkermansia*, *Lactobacillus* and *Roseburia* (**j**). Data represent the mean ± s.e.m. from a representative experiment ($n = 3$ (**a**–**c**), 4 (**f**) and 5 (**g**–**j**) biologically independent samples) of three (**a**–**c**) or two (**d**–**j**) independent experiments. Data were analysed using a two-way ANOVA (**e**), one-way ANOVA with Bonferroni's multiple comparisons test (**j**) or analysis of molecular variance test (**h**).

CT26 tumour re-challenge performed on day 62 (Fig. 5i), indicating a long-term memory response.

**The interplay between the gut microbiota, metabolites and stem-like memory CD8⁺ T cells.** We sought to delineate factors contributing to the systemic antitumour efficacy of the inulin gel plus α-PD-1 combination therapy. Tumour-bearing mice given inulin gel plus α-PD-1 failed to inhibit tumour growth after the administration of depletion antibody against CD8⁺ T cells (Fig. 6a), but not CD4⁺ T cells or natural killer (NK) cells, indicating CD8⁺ T cells as the major antitumour effector cells. In addition, broad-spectrum antibiotics added to the drinking water abrogated the antitumour effects of the inulin gel plus α-PD-1 therapy (Fig. 6b), suggesting the gut commensal microorganisms as a crucial link.

We next examined how the commensal microorganisms and their metabolites impact CD8⁺ T-cell responses. Therapy with inulin gel plus α-PD-1 increased the concentrations of SCFAs in the tumour-bearing mice (Fig. 6c). The G protein-coupled receptor 43 (GPR43, known as a key SCFA receptor in the gastrointestinal tract[23])-knockout mice that were treated with the inulin gel plus α-PD-1 combination therapy lost their ability to exert antitumour efficacy, increase CD8⁺ T-cell responses and decrease PD-1⁺CD8⁺ T cells in mesenteric lymph nodes (Fig. 6d,e), suggesting the importance of microbial fermentation-derived SCFAs. However, oral administration of free SCFAs failed to improve the antitumour efficacy of α-PD-1 IgG (Supplementary Fig. 13), probably due to the rapid absorption of SCFAs in the small intestine[24]. Together, these results suggest that SCFAs derived from microbial fermentation of inulin gel trigger GPR43-dependent, antitumour CD8⁺ T-cell responses.

When added to in vitro cultures of major histocompatibility complex (MHC) class I-restricted, ovalbumin (OVA)-specific, CD8⁺ T cells (OT-I CD8⁺ T cells) for either three or six days, SCFAs (acetate, propionate and butyrate) significantly augmented the IFN-γ recall response among memory OT-I CD8⁺ T cells (Fig. 7a)[25,26]. Importantly, SCFAs induced robust upregulation of T-cell

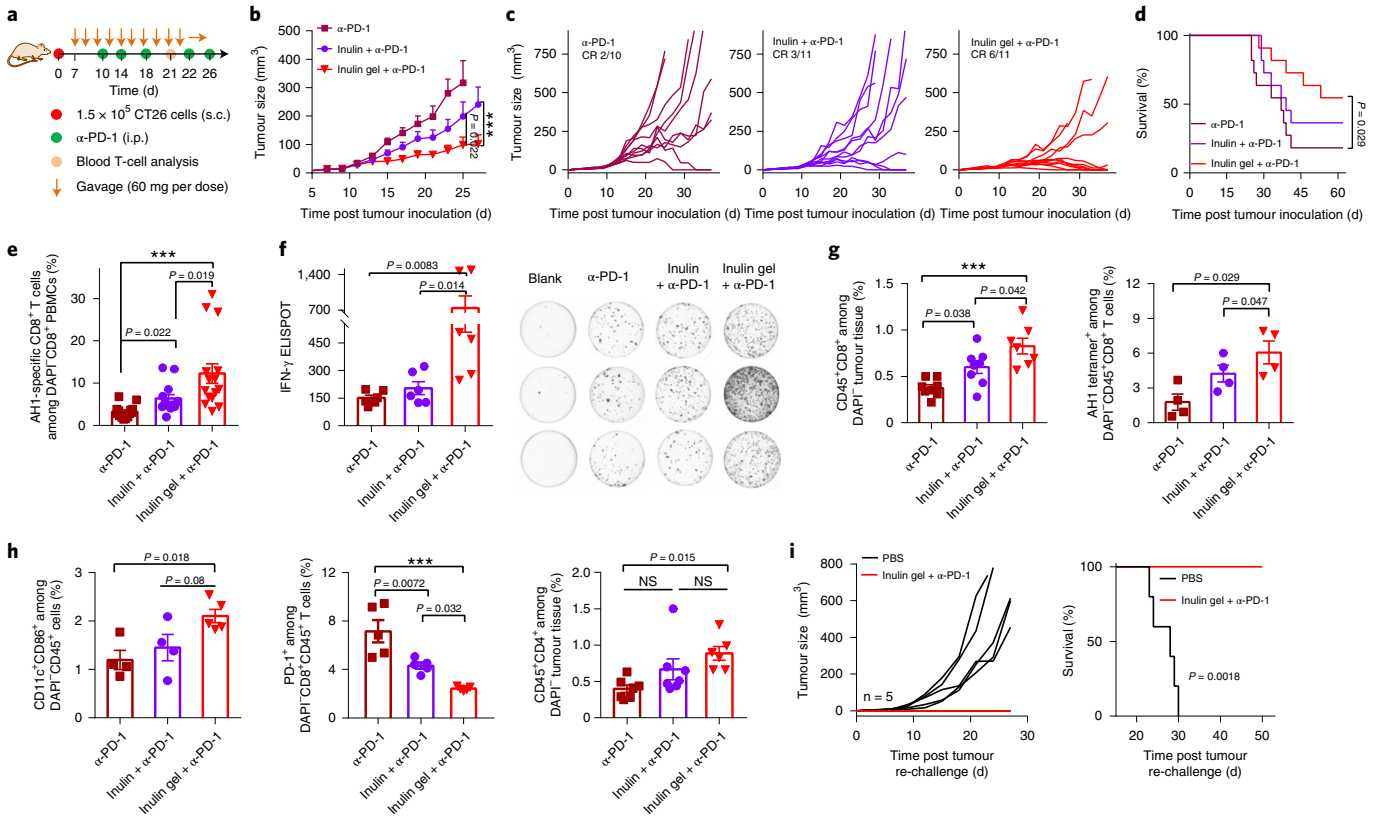


**Fig. 5 | Oral inulin gel potently amplifies the therapeutic efficacy of α-PD-1 therapy. a**, Therapeutic treatment regimen. CT26 tumour-bearing BALB/c mice were treated with inulin or inulin gel (60 mg per dose) starting on day 7, followed by α-PD-1 treatment as indicated. **b**–**d**, Average tumour growth (**b**), individual tumour growth (**c**) and overall Kaplan–Meier survival curves (**d**) for the experiment in **a**. **e**,**f**, Average frequency of AH1-specific CD8$^+$ T cells on day 21 (**e**) and AH1-specific IFN-γ enzyme-linked immune absorbent spot (ELISPOT) assay on splenocytes isolated on day 23 (**f**). **g**,**h**, The tumour tissues were analysed for the frequencies CD8$^+$ and AH1-tetramer$^+$CD8$^+$ T cells (**g**) as well as CD11c$^+$CD86$^+$ dendritic cells and PD-1$^+$CD8$^+$ and CD4$^+$ T cells (**h**). **i**, The survivors in the inulin gel plus α-PD-1 group were re-challenged with $1.5\times10^5$ CT26 cells s.c. inoculated on the contralateral flank on day 62, followed by tumour monitoring. Data represent the mean ± s.e.m. from a representative experiment ($n=10$ or 11 (**b**–**e**), 4–7 (**f**–**h**) and 5 (**i**) biologically independent animals) of three (**b**,**c**) or two (**d**–**i**) independent experiments. ***$P<0.001$; NS, not significant. Data were analysed using a one-way ANOVA (**e**–**h**) or two-way (**b**) ANOVA with Bonferroni's multiple comparisons test, or a log-rank (Mantel–Cox) test (**d**,**i**).

factor-1 (Tcf1, encoded by *Tcf7*; Fig. 7b and Supplementary Fig. 14). In agreement with these in vitro results, treatment of CT26 tumour-bearing mice with inulin gel plus α-PD-1 elicited substantially higher frequencies of CD44$^+$CD62L$^+$CD8$^+$ memory T cells in PBMCs as well as Tcf1$^+$CD8$^+$ and Tcf1$^+$PD-1$^+$CD8$^+$ T cells within the tumour microenvironment, tumour-draining lymph nodes (tdLNs) and non-tdLNs (Fig. 7c–f). Notably, Tcf1$^+$PD-1$^+$CD8$^+$ T cells, which are a progenitor stem-like subset of PD-1$^+$CD8$^+$ T cells, are associated with clinical responses to α-PD-1 ICB therapy in patients[27–29]. The inulin gel plus α-PD-1 treatment also increased the intratumoral concentrations of IFN-γ, interferon-inducible chemokine (C-X-C motif) ligand 9 (CXCL9) and the frequencies of CD3$^-$CD49b$^+$ NK cells and Ly6G$^+$CD11b$^+$ neutrophils, while inducing M1-skewed polarization of macrophages and reducing CD4$^+$CD25$^+$Foxp3$^+$ regulatory T cells (Fig. 7g–l and Supplementary Fig. 15). In addition, the mice that were treated with inulin gel plus α-PD-1 maintained normal complete blood counts and serum biochemistry (Supplementary Fig. 16), indicating the safety of the combination therapy. Although we mainly focused on the role of SCFAs in our current study, we also detected changes in other metabolites in faeces. Among the 255 metabolites that we measured, the inulin gel plus α-PD-1 therapy substantially increased the levels of hippurate, 1-methyl-L-histine, 3-methyl-L-histine, L-arginine and oleate (Fig. 7m). Interestingly, these metabolites have been reported to be associated with clinical responders to α-PD-1 IgG therapy[30].

**Therapeutic efficacy in multiple murine tumour models.** We sought to validate our results in mice obtained from different vendors, given that a recent report suggested that mice from various vendors harbour distinct commensal microbiota and respond differently to α-PD-1 therapy[8]. In alignment with the results obtained from CT26 tumour-bearing BALB/c mice (Jackson Laboratory), the inulin gel plus α-PD-1 combination therapy exerted a strong antitumour efficacy in the mice obtained from Charles River and Taconic Farm (Fig. 8a), thus ruling out vendor-specific effects. In addition, inulin gel also notably augmented the antitumour efficacy of the α-PD-1 and anti-cytotoxic T-lymphocyte-associated protein 4 (α-CTLA-4) combination therapy, leading to the regression of CT26 tumours in the BALB/c mice (Fig. 8b). Furthermore, the inulin gel plus α-PD-1 combination therapy also generated strong CD8$^+$ T-cell responses with robust antitumour efficacy in C57BL/6 mice (Jackson Laboratory) bearing either MC-38 colon carcinoma or B16F10 melanoma (Fig. 8c,d), thus showing utility of our strategy in murine models of colorectal carcinoma and melanoma using multiple mouse strains. Finally, in a transgenic mouse model of colorectal cancer[31], the inulin gel plus α-PD-1 combination therapy

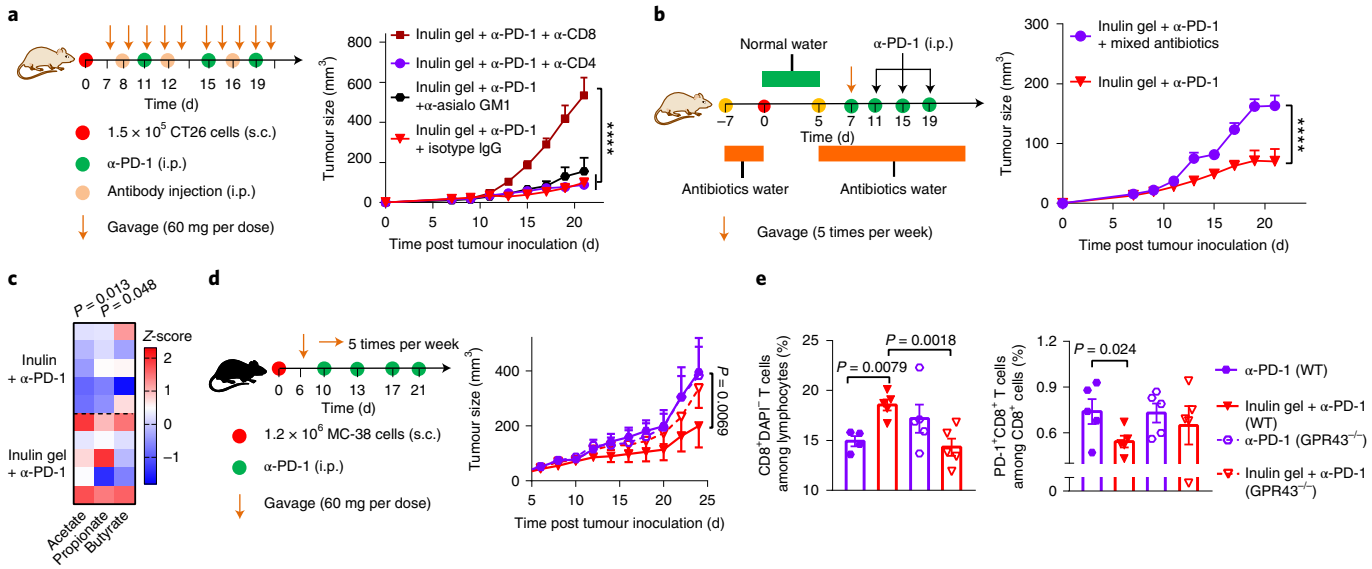


**Fig. 6 | The interplay between the gut microbiota, metabolites and antitumour efficacy. a**, CT26 tumour-bearing BALB/c mice were treated as shown (left) and i.p. administered with 200 μg of antibodies against CD8$^+$ T (α-CD8), CD4$^+$ T (α-CD4) or NK (α-asialo GM1) cells, or isotype IgG control on days 8, 12 and 16. The average tumour growth curves are shown (right). **b**, Broad-spectrum antibiotic (ampicillin, colistin and streptomycin) treatment regimen in the CT26 tumour model during therapy (left). The average tumour growth curves are shown (right). **c**, CT26 tumour-bearing BALB/c mice were treated as in Fig. 5a. The normalized *Z*-score values of SCFAs in the faeces of the mice on day 21 are shown. **d**,**e**, MC-38 tumour-bearing *GPR43* knockout (*GPR43*$^{-/-}$) or wild-type (WT) C57BL/6N mice were treated as shown (**d**, left). The mice were monitored for tumour growth (**d**, right) and the frequencies of CD8$^+$ and PD-1$^+$CD8$^+$ T cells in mesenteric lymph nodes were assessed on day 24 (**e**). Data represent the mean ± s.e.m. from a representative experiment ($n = 5$ biologically independent animals) from two (**a**,**b**,**d**,**e**) or three (**c**) independent experiments. ****$P < 0.0001$. Data were analysed using a one-way ANOVA (**e**) or two-way (**a**,**b**,**d**) ANOVA with Bonferroni's multiple comparisons test, or a two-tailed unpaired Student's *t*-test (**c**).

inhibited the growth of dextran sulfate sodium (DSS)-accelerated colon tumour formation in *CDX2–cre NLS–APC*$^{fl/fl}$ mice (Fig. 8e).

## Discussion

In summary, we have shown that inulin, a widely consumed dietary fibre with a long history of safety, synergizes with α-PD-1 therapy and elicits memory CD8$^+$ T-cell responses with robust antitumour efficacy (Fig. 2). We have also demonstrated that inulin formed into a hydrogel improves colon retention (Fig. 4d–f), modulates commensal microorganisms in situ (Fig. 4g–j) and further amplifies the antitumour efficacy of α-PD-1 therapy (Figs. 5 and 8). Mechanistically, our results suggest that the SCFAs produced as metabolites from inulin gel increase the memory potential of antigen-primed CD8$^+$ T cells and trigger their differentiation into stem-like Tcf1$^+$PD-1$^+$CD8$^+$ T cells (Fig. 7a–f), leading to potent long-lived antitumour effects. These results are in line with recent clinical studies showing that the concentrations of SCFAs are positively associated with the efficacy of ICB therapy in patients[32,33]. Interestingly, it was recently reported that mice kept on a high-dose free inulin diet (daily dose of approximately 450 mg) for 14 days before tumour inoculation could slow down tumour growth, but this did not synergize with α-PD-1 therapy[34], potentially due to decreased gut microbiota diversity triggered by the monotonous diet with very high inulin intake[35,36]. In contrast, we have shown that oral colon-retentive inulin gel given at intermittent doses of 60 mg potently amplifies the efficacy of α-PD-1 therapy in a therapeutic setting. Thus, in addition to FMT and consortia of probiotics currently being considered for improving cancer immunotherapies[37,38], our dietary fibre gel-based approach offers a powerful, safe and facile strategy for augmenting immune-checkpoint therapies.

Although biomaterials have been extensively explored for various therapeutic applications, the biomaterial described here is unique in that it is engineered to target and manipulate the gut microbiota in situ to promote systemic immunity. The oral hydrogel strategy outlined here represents a straightforward pathway to improve ICBs with minimal dose and favourable safety profiles. Notably, the recommended daily intake of dietary fibre is 25–38 g for adults, and the mean dietary fibre intake is only 15 g in the United States[39], thus leaving much room for dietary fibre-based therapeutics. As dysregulated gut microbiota and their metabolites have now been implicated in inflammatory, metabolic and neurodegenerative diseases, our strategy may provide a general framework for safely modulating the gut microbiome for the treatment of various diseases.

## Methods

**Preparation and characterization of inulin gel.** To prepare inulin gel, 300 mg of inulin from chicory (Sigma-Aldrich) was dissolved in 1.0 ml deionized water. The inulin solution was heated to 70 °C for 5 min and kept at room temperature for 12 h. For scanning-electron-microscope observation, the inulin gel was plunged into liquid nitrogen and the frozen sample was freeze-dried. The sample was then sputter coated with gold for 30 s. The samples were visualized using a MIRA3 TESCAN microscope (voltage 15 kV) at the Michigan Center for Materials Characterization at the University of Michigan. The rheology study of inulin gel was conducted in 25-mm sandblasted parallel plates with a Peltier temperature-controlled plate and hood (Anton Parr MCR702 Rheometer).

**In vivo cancer immunotherapy.** Animals were cared for following the federal, state and local guidelines. The University of Michigan, Ann Arbor is an AAALAC international accredited institution, and all work conducted on animals was in accordance with and approved by the Institutional Animal Care and Use Committee (IACUC). Female (6–8 weeks old) BALB/c mice from Jackson Laboratory, Charles Rivers or Taconic Farm maintained on normal mouse chow diet were inoculated with $1.5 \times 10^5$ CT26 cells per mouse, whereas C57BL/6 mice (Jackson Laboratory) were inoculated with $1.2 \times 10^6$ MC-38 or $3 \times 10^5$ B16F10 cells per mouse on the right flank by s.c. injection. The normal chow included 24.1% protein, 11.4% fat, 5.2% crude fibre, 48.7% nitrogen-free extract, 6.9% ash and less than 12.0% moisture (PicoLab Laboratory Rodent Diet 5L0D*, Lab Supply). Tumour-bearing mice were randomly assigned to different treatment groups. For the prophylactic antitumour studies in the CT26 tumour model, the mice were gavaged with melatonin (dose of 100 mg kg$^{-1}$ body weight; Alfa Aesar),

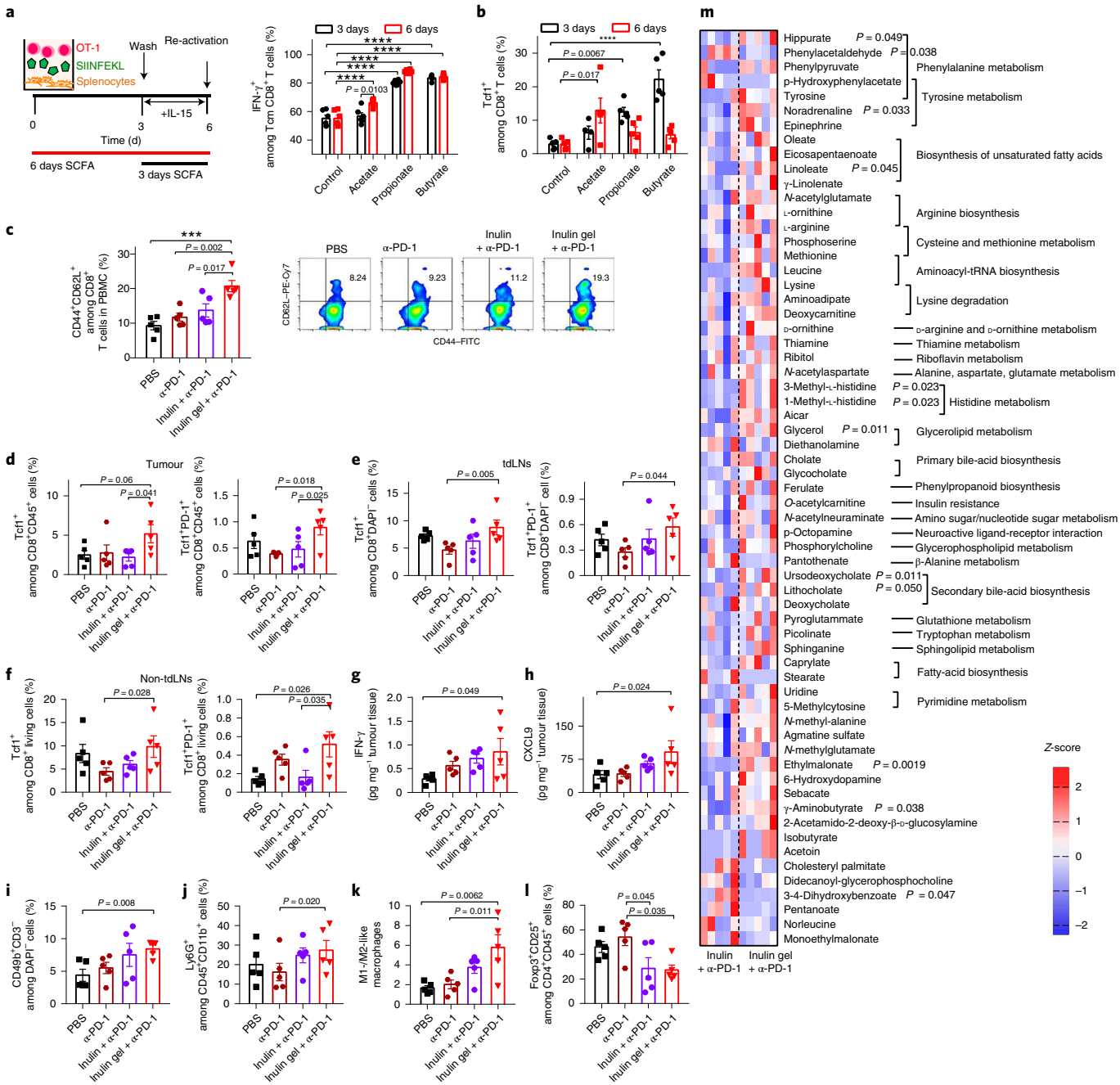


**Fig. 7 | The interplay between the gut microbiota, metabolites and induction of stem-like memory CD8⁺ T cells. a**,**b**, SCFAs (400 μM) were added during the in vitro memory differentiation of OVA-specific OT-I T cells. Frequencies of IFN-γ⁺ CD44⁺CD62L⁺ central memory (Tcm) CD8⁺ T cells (**a**) and the frequency of Tcf1 expression in CD8⁺ T cells after T-cell activation (**b**). **c**–**m**, CT26 tumour-bearing mice were treated as in Fig. 5a. **c**, Peripheral blood was analysed on day 19 for the frequency of CD44⁺CD62L⁺ Tcm CD8⁺ T cells. Representative flow cytometry plots with the percentage of cells in the top-right quadrant are shown (right). **d**–**f**, Tumour tissues (**d**), tdLNs (**e**) and non-tdLNs (**f**) were analysed on day 21 for the frequencies of the Tcf1⁺ and Tcf1⁺PD-1⁺ subsets of CD45⁺CD8⁺ T cells. **g**–**l**, Levels of IFN-γ (**g**) and CXCL9 (**h**), frequencies of CD3⁻CD49b⁺ NK cells (**i**) and Ly6G⁺CD11b⁺ neutrophils (**j**), ratio between M1- and M2-like macrophages (**k**), and frequency of Foxp3⁺CD25⁺ regulatory T cells on day 21 (**l**). **m**, Metabolites detected in faeces; 255 metabolites were measured in the faeces of the mice on day 21. Heatmap of the normalized *Z*-score values of discriminative metabolites. Data represent the mean ± s.e.m. from a representative experiment ($n = 6$ (**a**,**b**) and 5 (**c**–**m**) biologically independent samples) from three (**a**,**b**) or two (**c**–**m**) independent experiments. $^{***}P < 0.001$, $^{****}P < 0.0001$. Data were analysed using a one-way ANOVA (**c**–**l**) or two-way ANOVA (**a**,**b**) with Bonferroni's multiple comparisons test, or a two-tailed unpaired Student's *t*-test (**m**).

EGCG (dose of 100 mg kg$^{-1}$ body weight; Sigma-Aldrich), fucoidan from *Fucus vesiculosus* (dose of 200 mg kg$^{-1}$ body weight; Sigma-Aldrich), FOS from chicory (120 mg per dose; Sigma-Aldrich) or inulin (120 mg per dose) three times in one week before the tumour inoculation. After the tumour inoculation, the mice were gavaged three times in the first week, followed by five times a week. The mice were i.p. injected with α-PD-1 antibody (100 μg per dose; clone RMP1-14, Bioxcell) on days 10, 14, 18 and 22 post tumour inoculation. For combination therapies in the CT26 tumour model, the mice were gavaged with the indicated samples from day 7 post tumour inoculation. The mice were gavaged with the indicated samples (same dose as in the prophylactic antitumour studies) five times per week and

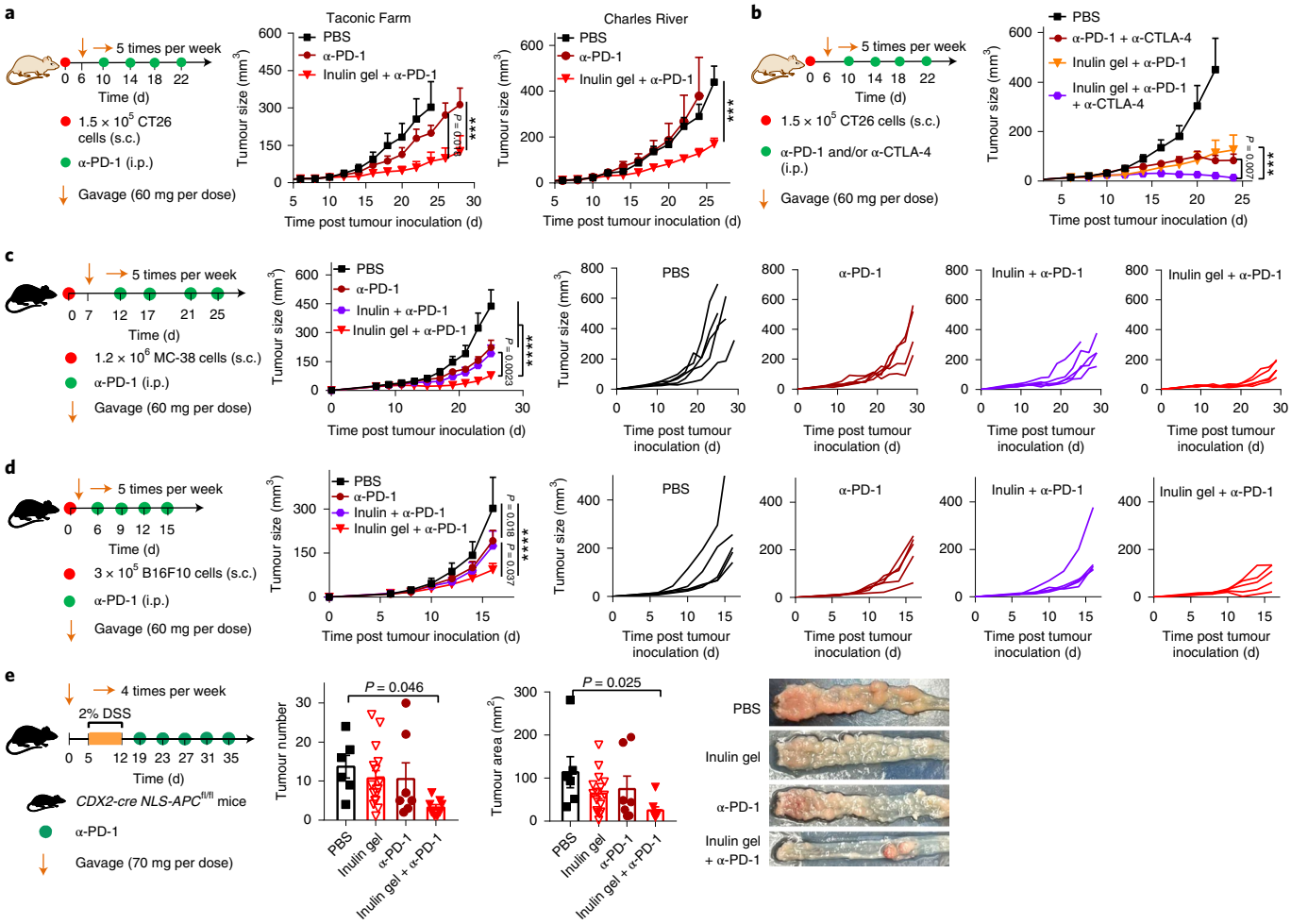


**Fig. 8 | Therapeutic efficacy of inulin gel plus α-PD-1 therapy in multiple tumour models. a**, CT26 tumour-bearing BALB/c mice from Taconic Farm or Charles River were treated as shown (left; inulin, 60 mg per dose) and tumour growth was monitored (right). **b**, CT26 tumour-bearing BALB/c mice from Jackson Laboratory were treated with inulin gel with or without α-PD-1 and α-CTLA-4 as shown (left), and tumour growth was monitored (right). **c**,**d**, C57BL/6 mice bearing MC-38 colon carcinoma (**c**) or B16F10 melanoma (**d**) were treated as shown (left; inulin, 60 mg per dose), and the average tumour growth was monitored (middle). Tumour growth for individual mice in each treatment group following tumour inoculation is shown (right). **e**, *CDX2-cre NLS-APC*$^{fl/fl}$ mice were provided with 2% DSS in their drinking water for one week to promote the formation of tumours in the colon and then treated as indicated (left). Three of the nine mice in the PBS group, two of the 17 mice in the inulin-gel group and one of the eight mice in the α-PD-1 group were euthanized due to a severe decrease in their body weight or rectal bleeding/prolapse. On day 45, the number and size of the colon tumours were measured for the survivors (middle). Representative images of the colon tissue are shown (right). Data represent the mean ± s.e.m. from a representative experiment ($n = 5$ (**a**–**d**) and 8 or 9 (**e**) biologically independent animals) from two independent experiments. ***$P < 0.001$, ****$P < 0.0001$. Data were analysed using a two-way ANOVA (**a**–**d**) or one-way ANOVA (**e**) with Bonferroni's multiple comparisons test.

α-PD-1 antibody (100 μg per dose) was i.p. injected on days 11, 15, 19 and 23. For inulin-gel combination therapy in the CT26 tumour model, inulin gel or inulin was used at a dose of 30, 60 or 120 mg; and the α-PD-1 antibody (100 μg per dose) was i.p. injected on days 10, 14, 18, 22 and 26. For the α-CTLA-4 combination therapy in the CT26 tumour model, inulin gel or inulin was used at 60 mg per dose, and the α-PD-1 (100 μg per dose) and α-CTLA-4 (100 μg per dose; clone 9D9, Bioxcell) antibodies were i.p. injected on days 10, 14, 18 and 22. For the *GPR43*$^{-/-}$ mice study, *GPR43*$^{-/-}$ or wild-type C57BL/6N male mice were inoculated with $1.2 \times 10^6$ MC-38 cells per mouse on the right flank by s.c. injection. The mice were gavaged with inulin gel (60 mg per dose) and α-PD-1 antibody (100 μg per dose) was i.p. injected on days 10, 13, 17 and 21. For spontaneous colorectal cancer therapy, 6–8-week-old *CDX2–cre NLS–APC*$^{fl/fl}$ mice were orally gavaged with inulin gel (70 mg per dose) four times per week. The mice were given 2% DSS ($M_w$, 4 kDa; Alfa Aesar) in their drinking water from days 5 to 12 and α-PD-1 antibody (100 μg per dose) was i.p. injected on days 19, 23, 27, 31 and 35. The mice were euthanized on day 45 and the colon tumours were counted and measured under a magnifier. For the SCFA plus α-PD-1 study in the CT26 tumour model, the drinking water was supplemented with 120 mM sodium chloride or a mixture of 65 mM sodium acetate, 25 mM sodium propionate and 30 mM sodium butyrate; α-PD-1 (100 μg per dose) injection was performed on days 11, 14, 17 and 20. The tumour size was measured and the tumour volume was calculated as ½ × (length × width$^2$). Tumour-bearing mice were euthanized when the tumour size reached 1.5 cm in any diameter or when the animals became moribund with severe weight loss (>20%) or tumour ulceration. For the immune cell-depletion studies, depletion antibodies (200 μg per dose) against anti-CD8 (clone 2.43; Bioxcell, cat. no. BP0061), anti-CD4 (clone GK1.5; Bioxcell, cat. no. BP0003-1) or anti-asialo GM1 (Wako chemicals USA, Inc, cat. no. 986-10001) were administered i.p. on days 8, 12 and 16 post tumour inoculation and treated as above.

**In vivo immunological analyses.** We analysed PBMCs for the tumour antigen-specific CD8$^+$ T cells. Red blood cells were lysed and discarded, and the remaining cells were blocked with CD16/32 antibody for 10 min and then stained with PE-tagged peptide-MHC tetramer (H-2L$^d$-restricted SPSYVYHQF). Tetramers were provided by the NIH Tetramer Core Facility. The cells were further stained with APC–CD8 rat anti-mouse (clone 53-6.7(RUO); BD Biosciences). To further analyse the memory phenotype of tetramer$^+$ CD8$^+$ T cells, the cells were additionally stained with FITC–CD44 rat anti-human/mouse (clone IM7; eBioscience) and PE-Cy7–CD62L monoclonal antibody (clone MEL-14;

eBioscience). The stained cells were incubated with 4′,6-diamidino-2-phenylindole (DAPI) before flow cytometry analysis. For the lymph-node tissue analysis, tdLNs, non-tdLNs and mesenteric lymph nodes were isolated, ground and filtered through a 70-μm strainer. The cells were stained with the designated antibodies as well as the fixable viability dye eFluor 450 (eBioscience) for flow cytometry analysis. Tumour tissues were excised at preset time points for analysis of the tumour-infiltrating T cells. The tumour tissues were weighed, cut into small pieces and incubated with collagenase type IV (1 mg ml$^{-1}$) and DNase I (0.1 mg ml$^{-1}$) under gentle shaking. After 30 min, the cell suspension was filtered through a 70-μm strainer. The filtrate was diluted with PBS to 3 ml and chemokines/cytokines were detected via enzyme-linked immunosorbent assay by the Cancer Center Immunology Core of the University of Michigan. The cells were washed with fluorescence-activated cell sorting (FACS) buffer and blocked with CD16/32 antibody. The cells were then stained with the designated antibodies: PE–CD4 monoclonal antibody (clone GK1.5; eBioscience), APC–anti-CD45 rat monoclonal antibody (clone 30-F11; BioLegend), FITC–anti-CD45 rat monoclonal antibody (clone 30-F11; BioLegend), FITC–rat anti-mouse CD8 (clone 53-6.7(RUO); BD Biosciences), PE-labelled H-2L$^{d}$-restricted SPSYVYHQF, FITC–anti-CD86 rat monoclonal antibody (clone GL-1; BioLegend), PE–CD11c Armenian hamster anti-mouse (clone N418; eBioscience), PE-Cy7–anti-mouse PD-1 (clone 29F.1A12; BioLegend), PE–Tcf1/Tcf7 rabbit monoclonal antibody (clone C63D9; Cell Signaling Technology), PE-Cy7–anti-mouse CD86 (clone GL1; BD Bioscience), FITC–anti-mouse/human CD11b (clone M1/70; BioLegend), PE–anti-mouse F4/80 (clone BM8; BioLegend), APC–anti-mouse CD206 (MMR; clone C068C2; BioLegend), PE–Foxp3 monoclonal antibody (clone FJK-16s; eBioscience), APC–CD25 rat anti-mouse (clone PC61; BD Biosciences), FITC–anti-CD49b rat monoclonal antibody (clone DX5; BioLegend), Brilliant Violet 786-CD3 molecular complex rat anti-mouse (clone 17A2; BD Biosciences), FITC–CD279 (PD-1) rat anti-mouse (clone RMP1 30; eBioscience) and PE–Ly6G monoclonal antibody (clone 1A8-Ly6g; eBioscience). The cells were washed and stained with DAPI, 7-aminoactinomycin D or the fixable viability dye eFluor 450 (eBioscience) for flow cytometric analysis. For the IFN-γ ELISPOT assay, an ELISPOT plate was coated with IFN-γ capture antibody for 24 h and blocked with DMEM medium containing 10% fetal bovine serum for 2 h. Splenocytes obtained from the pretreated mice were added to a 96-well plate at a concentration of $2\times10^{5}$ live cells per well. SPSYVYHQF peptide (20 μg ml$^{-1}$) was added to stimulate the splenocytes. Ionomycin and phorbol myristate acetate were employed as the positive control. After 18 h, the IFN-γ spots were detected with biotinylated detection antibody, followed by streptavidin–horseradish peroxidase and AEC substrate kit. The number and size of the IFN-γ spots were measured by the Cancer Center Immunology Core at the University of Michigan.

**Microbial community analyses.** CT26 tumour-bearing BALB/c mice were treated as the described earlier; faecal pellets were collected on day 21 and stored at −80 °C before microbial analysis. Microbiome DNA isolation and 16S rRNA gene sequencing were completed by the Microbial Systems Molecular Biology Laboratory at the University of Michigan. Isolation of microbial DNA from the faeces of the mice was performed using a Qiagen MagAttract power microbiome kit. The V4 region of the 16S rRNA-encoding gene was amplified from extracted DNA using the barcoded dual-index primers. Briefly, barcoded dual-index primers specific to the V4 region of the 16S rRNA gene amplified the DNA. The PCR was conducted in the following order: 2 min at 95 °C; 30 cycles of 95 °C for 20 s, 55 °C for 15 s, 72 °C for 5 min; and 72 °C for 10 min. The size of the amplicon library (approximately 399 bp) was confirmed using an Agilent Bioanalyzer.
The pooled amplicon library was then sequenced on the Illumina MiSeq platform using the 500-cycle MiSeq V2 reagent kit (cat. no. MS-102-2003) according to the manufacturer's instructions, with modifications of the primer set with custom read 1/read 2 and index primers added to the reagent cartridge. The 'Preparing Libraries for Sequencing on the MiSeq' (part 15039740, Rev. D) protocol was used to prepare libraries with a final load concentration of 5.5 pM, spiked with 15% PhiX to create diversity within the run. FASTQ files were obtained when the $2\times250$ bp sequencing completed. The raw microbial 16S rRNA gene sequencing data were analysed using Mothur (mothur v.1.40.5; running 64-Bit Version). Silva reference files (release 132) were used to align sequences and the open reference OTU picking protocol was used at 97% sequence identity. The data processing steps based on the MiSeq standard operating procedure[40] included reducing sequencing and PCR errors, processing improved sequences (align and filter the sequences to remove the overhangs at both ends, de-noise sequences and remove chimaeric sequences, undesirables and so on), assessing error rates, preparing for analysis, analysis and OTU-based analysis. The pcr.seqs command aligns sequences to the reference (silva.nr_v132.align) alignment. For classifying sequences, Bayesian classifier with the classify.seqs command was used with a cutoff of 80; silva.nr_v132.align and silva.nr_v132.tax were used as the reference and taxonomy, respectively.

**Quantification of faecal pH, SCFAs and other metabolites.** Fresh mouse faecal pellets were collected and weighed on day 21 post tumour inoculation and treatment. The faecal pellets were homogenized in deionized water and centrifuged at 3,000*g* for 5 min. The pH of the supernatant was detected using a pH meter.

For the SCFA measurements, SCFAs were extracted from the faecal pellets using Milli-Q water. The solution was centrifuged for 5 min at 10,000*g* (4 °C) to pellet bacteria and other solids. The supernatant was collected and the SCFAs were analysed using a Dionex Integrion high performance ion chromatography system outfitted with an AS-11HC column (250 mm × 4 mm ID; 4 μm packing) by the University of Michigan Biological Station. The separation was accomplished through the use of a hydroxide gradient (1–5 mM over the course of 20 min, followed by a rapid ramp to 60 mM to clear the column of anions); the detection was conducted under suppressed conductivity. To measure other metabolites, chilled methanol–water solution (80% MeOH vol/vol) was added to the faeces (1 g faeces to 10 ml solution). The mixture was vortexed in a cold room for 20 min, followed by centrifugation at 17,000*g* for 20 min at 4 °C. The supernatant was collected in fresh tubes, dried in a vacuum evaporator and stored at −80 °C. The dried supernatant was reconstituted in 300 μl water, sonicated for 20 min and then filtered. The filtrate (100 μl) was transferred to liquid-chromatography vials and analysed on an Agilent 6520 QTOF LC/mass spectrometry machine using an ACQUITY UPLC BEH C18 column, 130 Å, 1.7 μm, 2.1 mm × 150 mm coupled with Van-Guard pre-columns. The column compartment was set at 40 °C and the analysis was performed in both positive and negative modes. Mobile phase A was water with 0.1% formic acid, and mobile phase B was acetonitrile with 0.1% formic acid. The gradient method was set as follows: 0 min, 1% phase B; 1 min, 1% phase B; 8 min, 99% phase B; 13 min, 85% phase B; 13.1 min, 1% phase B; and 16 min, 1% phase B. The metabolite peaks were extracted using Agilent Masshunter Profinder based on our in-house library. Any metabolites with a relative standard deviation greater than 30% in the quality-control measurements were removed from further analysis. The peak areas were normalized to the weight of the faecal matter. Pathway analysis was performed using Metaboanalyst.

**Retention of inulin gel in the gastrointestinal system.** To prepare FITC-tagged inulin gel, 47.5 mg inulin and 12.5 mg FITC–inulin (Sigma-Aldrich) were mixed in 200 μl deionized water, followed by inulin-gel formation as described in the 'Preparation and characterization of inulin gel' section. A mixture of 47.5 mg inulin and 12.5 mg FITC–inulin was used as the soluble FITC–inulin control. For in vivo imaging, the mice were gavaged with FITC-tagged inulin or inulin gel and euthanized at preset time points (2, 4.5, 7, 9.5 and 12 h). The stomach, small intestine, caecum, colon and rectum were harvested, washed briefly with PBS and visualized using the IVIS optical imaging system. To detect the inulin content in the colon, the mice were gavaged with inulin or inulin gel (60 mg per dose) and euthanized at preset times (2, 4.5, 7, 9.5 and 12 h) post gavage. The digesta in the colon was harvested, weighed and added to 1.5 ml deionized water. The samples were homogenized and centrifuged, and the supernatants were diluted 20 times for quantification of the inulin content using the PicoProbe inulin assay kit (BioVision) according to the manufacturer's instructions.

**Antibiotic treatment.** BALB/c mice were pretreated with sterile drinking water containing antibiotics (0.3 mg ml$^{-1}$ ampicillin, 2.5 mg ml$^{-1}$ streptomycin and 0.3 mg ml$^{-1}$ colistin) for 7 days. After tumour inoculation on day 0, the mice were provided with sterile drinking water for 5 days to avoid any potential effects of antibiotics on tumour engraftment and formation. Starting on day 5, antibiotics were added to the drinking water throughout the remainder of the study. The antibiotic drinking water was replaced twice a week. The dilatation of the caecum was observed to confirm the antibiotic activity. Gavage with inulin gel (60 mg per dose) began from day 7 and α-PD-1 was injected on days 11, 15 and 19.

**In vitro stimulation of OT-I T cells with SCFAs.** Splenocytes from OT-I mice were obtained aseptically. The cells were cultured in 96-well plates ($1\times10^{5}$ cells per well) and activated with SIINFEKL peptide ($4\times10^{-9}$ M) in the presence or absence of SCFAs (400 μM) for 3 days. Then cells were washed three times with T-cell medium and further cultured with interleukin-15 (10 ng ml$^{-1}$; PeproTech) in the presence or absence of SCFAs for 3 days to generate OVA-specific OT-I memory CD8$^{+}$ T cells. The cells were then washed twice and re-activated with SIINFEKL peptide (10 μM) for 2 h. Subsequently, brefeldin A was added (1:1,000 dilution) and incubated for another 2 h. The suspension cells were collected, blocked with CD16/32 antibody and stained with the fixable viability dye eFluor 450, FITC–CD44 rat anti-human/mouse and PE-Cy7–CD62L monoclonal antibody. Intracellular IFN-γ (PE–anti-mouse IFN-γ, clone XMG1.2; BioLegend)- and Tcf1 (PE–Tcf1/Tcf7 rabbit monoclonal antibody)-positive T cells were detected via flow cytometry.

**Safety evaluation.** CT26 tumour-bearing mice were treated as in Fig. 5a. On day 29, blood was collected for a complete blood count (including eosinophil, lymphocyte, monocyte, platelet and red blood cell counts; haemoglobin, mean platelet volume, red-cell distribution width and mean corpuscular haemoglobin). Meanwhile, some blood was collected, solidified and centrifuged to obtain the serum for biochemical analysis: glutamic pyruvate transaminase, aspartate aminotransferase, blood urea nitrogen, glucose, cholesterol and creatine phosphokinase. The mice were euthanized on day 29. The lung, liver, spleen, heart and kidneys were collected for haematoxylin and eosin staining. All of these tests were performed at the In-Vivo Animal Core of the University of Michigan.

**Statistical analysis.** All experiments were performed at least twice with duplicate repeated measures. The results are expressed as the mean ± s.e.m. A one-way or two-way analysis of variance (ANOVA), followed by Bonferroni's multiple comparisons post hoc test was used for testing differences between groups. Data were approximately normally distributed and variance was similar between the groups. The experiments were repeated multiple times as independent experiments, as indicated in the figure captions. A complete dataset from one representative, independent experiment is shown in the figures. No samples were excluded from the analyses. Statistical significance is indicated as $^{*}P<0.05$, $^{**}P<0.01$, $^{***}P<0.001$ and $^{****}P<0.0001$. GraphPad Prism 8.0 (GraphPad Software) was used for the statistical analyses.

**Reporting Summary.** Further information on research design is available in the Nature Research Reporting Summary linked to this article.

## Data availability

The main data supporting the findings of this study are available within the paper and its Supplementary Information. The raw and analysed datasets generated during the study are too large to be publicly shared, but they are available for research purposes from the corresponding author on reasonable request. The bacterial 16S rRNA sequencing data have been deposited in the NCBI Sequence Read Archive (accession number: PRJNA715170).

Received: 18 September 2020; Accepted: 14 May 2021;
Published online: 24 June 2021

## References

1. Topalian, S. L., Taube, J. M., Anders, R. A. & Pardoll, D. M. Mechanism-driven biomarkers to guide immune checkpoint blockade in cancer therapy. *Nat. Rev. Cancer* **16**, 275–287 (2016).
2. Ribas, A. & Wolchok, J. D. Cancer immunotherapy using checkpoint blockade. *Science* **359**, 1350–1355 (2018).
3. Lynch, S. V. & Pedersen, O. The human intestinal microbiome in health and disease. *N. Engl. J. Med.* **375**, 2369–2379 (2016).
4. Gilbert, J. A. et al. Current understanding of the human microbiome. *Nat. Med.* **24**, 392–400 (2018).
5. Schmidt, T. S. B., Raes, J. & Bork, P. The human gut microbiome: from association to modulation. *Cell* **172**, 1198–1215 (2018).
6. Cryan, J. F., O'Riordan, K. J., Sandhu, K., Peterson, V. & Dinan, T. G. The gut microbiome in neurological disorders. *Lancet Neurol.* **19**, 179–194 (2020).
7. Vetizou, M. et al. Anticancer immunotherapy by CTLA-4 blockade relies on the gut microbiota. *Science* **350**, 1079–1084 (2015).
8. Sivan, A. et al. Commensal *Bifidobacterium* promotes antitumor immunity and facilitates anti-PD-L1 efficacy. *Science* **350**, 1084–1089 (2015).
9. Matson, V. et al. The commensal microbiome is associated with anti-PD-1 efficacy in metastatic melanoma patients. *Science* **359**, 104–108 (2018).
10. Routy, B. et al. Gut microbiome influences efficacy of PD-1-based immunotherapy against epithelial tumors. *Science* **359**, 91–97 (2018).
11. Gopalakrishnan, V. et al. Gut microbiome modulates response to anti-PD-1 immunotherapy in melanoma patients. *Science* **359**, 97–103 (2018).
12. Zitvogel, L., Ma, Y., Raoult, D., Kroemer, G. & Gajewski, T. F. The microbiome in cancer immunotherapy: diagnostic tools and therapeutic strategies. *Science* **359**, 1366–1370 (2018).
13. Helmink, B. A., Khan, M. W., Hermann, A., Gopalakrishnan, V. & Wargo, J. A. The microbiome, cancer, and cancer therapy. *Nat. Med.* **25**, 377–388 (2019).
14. Giles, E. M., D'Adamo, G. L. & Forster, S. C. The future of faecal transplants. *Nat. Rev. Microbiol.* **17**, 719 (2019).
15. Skelly, A. N., Sato, Y., Kearney, S. & Honda, K. Mining the microbiota for microbial and metabolite-based immunotherapies. *Nat. Rev. Immunol.* **19**, 305–323 (2019).
16. Wang, J., Man, G. C. W., Chan, T. H., Kwong, J. & Wang, C. C. A prodrug of green tea polyphenol (–)-epigallocatechin-3-gallate (Pro-EGCG) serves as a novel angiogenesis inhibitor in endometrial cancer. *Cancer Lett.* **412**, 10–20 (2018).
17. Makki, K., Deehan, E. C., Walter, J. & Bäckhed, F. The impact of dietary fiber on gut microbiota in host health and disease. *Cell Host Microbe* **23**, 705–715 (2018).
18. Paulose, J. K., Wright, J. M., Patel, A. G. & Cassone, V. M. Human gut bacteria are sensitive to melatonin and express endogenous circadian rhythmicity. *PLoS ONE* **11**, e0146643 (2016).
19. Stewart, M. L., Savarino, V. & Slavin, J. L. Assessment of dietary fiber fermentation: effect of *Lactobacillus reuteri* and reproducibility of short-chain fatty acid concentrations. *Mol. Nutr. Food Res.* **53**, S114–S120 (2009).
20. La Rosa, S. L. et al. The human gut Firmicute *Roseburia intestinalis* is a primary degrader of dietary β-mannans. *Nat. Commun.* **10**, 905 (2019).
21. Zhao, J. et al. Fiber-rich foods affected gut bacterial community and short-chain fatty acids production in pig model. *J. Funct. Foods* **57**, 266–274 (2019).
22. Cao, Y. & Mezzenga, R. Design principles of food gels. *Nat. Food* **1**, 106–118 (2020).
23. Sun, M. et al. Microbiota-derived short-chain fatty acids promote Th1 cell IL-10 production to maintain intestinal homeostasis. *Nat. Commun.* **9**, 3555 (2018).
24. de Groot, P. F. et al. Oral butyrate does not affect innate immunity and islet autoimmunity in individuals with longstanding type 1 diabetes: a randomised controlled trial. *Diabetologia* **63**, 597–610 (2020).
25. Balmer, M. L. et al. Memory $CD8^{+}$ T cells require increased concentrations of acetate induced by stress for optimal function. *Immunity* **44**, 1312–1324 (2016).
26. Bachem, A. et al. Microbiota-derived short-chain fatty acids promote the memory potential of antigen-activated $CD8^{+}$ T cells. *Immunity* **51**, 285–297 (2019).
27. Siddiqui, I. et al. Intratumoral $Tcf1^{+}$ $PD\text{-}1^{+}$ $CD8^{+}$ T cells with stem-like properties promote tumor control in response to vaccination and checkpoint blockade immunotherapy. *Immunity* **50**, 195–211 (2019).
28. Jansen, C. S. et al. An intra-tumoral niche maintains and differentiates stem-like CD8 T cells. *Nature* **576**, 465–470 (2019).
29. Sade-Feldman, M. et al. Defining T cell states associated with response to checkpoint immunotherapy in melanoma. *Cell* **175**, 998–1013 (2018).
30. Hatae, R. et al. Combination of host immune metabolic biomarkers for the PD-1 blockade cancer immunotherapy. *JCI Insight* **5**, e133501 (2020).
31. Hinoi, T. et al. Mouse model of colonic adenoma-carcinoma progression based on somatic *Apc* inactivation. *Cancer Res.* **67**, 9721–9730 (2007).
32. Nomura, M. et al. Association of short-chain fatty acids in the gut microbiome with clinical response to treatment with nivolumab or pembrolizumab in patients with solid cancer tumors. *JAMA Netw.* **3**, e202895 (2020).
33. Botticelli, A. et al. Gut metabolomics profiling of non-small cell lung cancer (NSCLC) patients under immunotherapy treatment. *J. Transl. Med.* **18**, 1–10 (2020).
34. Li, Y. et al. Prebiotic-induced anti-tumor immunity attenuates tumor growth. *Cell Rep.* **30**, 1753–1766 (2020).
35. Senghor, B., Sokhna, C., Ruimy, R. & Lagier, J.-C. Gut microbiota diversity according to dietary habits and geographical provenance. *Hum. Microbiome J.* **7–8**, 1–9 (2018).
36. Salgia, N. J. et al. Stool microbiome profiling of patients with metastatic renal cell carcinoma receiving anti–PD-1 immune checkpoint inhibitors. *Eur. Urol.* **78**, 498–502 (2020).
37. Derosa, L., Routy, B., Kroemer, G. & Zitvogel, L. The intestinal microbiota determines the clinical efficacy of immune checkpoint blockers targeting PD-1/PD-L1. *Oncoimmunology* **7**, e1434468 (2018).
38. Khan, M. A. W., Ologun, G., Arora, R., McQuade, J. L. & Wargo, J. A. Gut microbiome modulates response to cancer immunotherapy. *Dig. Dis. Sci.* **65**, 885–896 (2020).
39. King, D. E., Mainous, A. G. 3rd & Lambourne, C. A. Trends in dietary fiber intake in the United States, 1999–2008. *J. Acad. Nutr. Diet.* **112**, 642–648 (2012).
40. Kozich, J. J., Westcott, S. L., Baxter, N. T., Highlander, S. K. & Schloss, P. D. Development of a dual-index sequencing strategy and curation pipeline for analyzing amplicon sequence data on the MiSeq Illumina sequencing platform. *Appl. Environ. Microbiol.* **79**, 5112–5120 (2013).

## Acknowledgements

This work was supported by the NIH (grant nos R01AI127070, R01EB022563, R01CA210273, U01CA210152, R01DK125087, P30CA046592). J.J.M. is supported by an NSF CAREER Award (grant no. 1553831). D.N. is supported by NCI grant nos R01CA227622, R01CA222251 and R01CA204969; a Rogel Cancer Center grant and a Forbes Scholar Award. We acknowledge the NIH Tetramer Core Facility (contract HHSN272201300006C) for the provision of MHC-I tetramers and C. H. Kim for the provison of *GPR43*$^{-/-}$ mice. Opinions, interpretations, conclusions and recommendations are those of the author and are not necessarily endorsed by the Department of Defense. We thank M. E. Aikins for critical review of the manuscript, Y. Xu for ELISPOT tests, K. Saud for rheology tests, J. Lu for help with the microbiota data analysis and H. He for helping with the animal studies. Figure 1 was created by the authors using BioRender.com.

## Author contributions

K.H. and J.J.M. designed the study. K.H. and J.X. performed the experiments. J.N., X.S. and X.H. provided technical help with the flow cytometry, NMR and matrix-assisted laser desorption/ionization–time-of-flight analyses. A.A., O.A., J.H.J. and D.N. assisted with the measurement of metabolites. B.P. and G.Y.C. aided with the colon tumorigenesis study. N.K. assisted with the gut microbiome studies. K.H. and J.J.M. interpreted the data and wrote the paper.

## Competing interests

A patent application (WO/2021/061789) for in situ modulation of the gut microbiome has been filed, with J.J.M., K.H., J.X. and X. H. as inventors.

## Additional information

**Supplementary information** The online version contains supplementary material available at https://doi.org/10.1038/s41551-021-00749-2.

**Correspondence and requests for materials** should be addressed to J.J.M.

**Peer review information** *Nature Biomedical Engineering* thanks Bertrand Routy and the other, anonymous, reviewer(s) for their contribution to the peer review of this work.

nature research

Corresponding author(s): James J. Moon

Last updated by author(s): May 13, 2021

# Reporting Summary

Nature Research wishes to improve the reproducibility of the work that we publish. This form provides structure for consistency and transparency in reporting. For further information on Nature Research policies, see our Editorial Policies and the Editorial Policy Checklist.

## Statistics

For all statistical analyses, confirm that the following items are present in the figure legend, table legend, main text, or Methods section.

| n/a | Confirmed |
|---|---|
| ☐ | ☒ The exact sample size (*n*) for each experimental group/condition, given as a discrete number and unit of measurement |
| ☐ | ☒ A statement on whether measurements were taken from distinct samples or whether the same sample was measured repeatedly |
| ☐ | ☒ The statistical test(s) used AND whether they are one- or two-sided<br>*Only common tests should be described solely by name; describe more complex techniques in the Methods section.* |
| ☐ | ☒ A description of all covariates tested |
| ☐ | ☒ A description of any assumptions or corrections, such as tests of normality and adjustment for multiple comparisons |
| ☐ | ☒ A full description of the statistical parameters including central tendency (e.g. means) or other basic estimates (e.g. regression coefficient) AND variation (e.g. standard deviation) or associated estimates of uncertainty (e.g. confidence intervals) |
| ☐ | ☒ For null hypothesis testing, the test statistic (e.g. *F*, *t*, *r*) with confidence intervals, effect sizes, degrees of freedom and *P* value noted<br>*Give P values as exact values whenever suitable.* |
| ☒ | ☐ For Bayesian analysis, information on the choice of priors and Markov chain Monte Carlo settings |
| ☐ | ☒ For hierarchical and complex designs, identification of the appropriate level for tests and full reporting of outcomes |
| ☐ | ☒ Estimates of effect sizes (e.g. Cohen's *d*, Pearson's *r*), indicating how they were calculated |

*Our web collection on statistics for biologists contains articles on many of the points above.*

## Software and code

Policy information about availability of computer code

| | |
|---|---|
| Data collection | SEM images were acquired by using a MIRA3 TESCAN. Flow cytometric data were collected using BD FACSDiva (v.8.0.1). Microbiome data from feces were collected using the MiSeq Illumina sequencing platform. In vivo images were acquired using IVIS Lumina Living Image Software(v.4.5.5). 1HNMR data were acquired using an Agilent 400 MHz MR NMR spectrometer. |
| Data analysis | Flow-cytometry analysis was done in BD FACSDiva and FlowJo (v.10.5) (Tree Star). Microbiome analysis was done in the community-supported software program mothur (v.1.40.5) and by the steps in the MiSeq SOP (http://mothur.org/wiki/MiSeq_SOP). In vivo images were analysed using IVIS Lumina Living Image (v.4.5.5) Software. 1HNMR data were analysed using Mestrenova (v.14.1.0) software. Statistical analysis was done in GraphPad Prism 8.0. |

For manuscripts utilizing custom algorithms or software that are central to the research but not yet described in published literature, software must be made available to editors and reviewers. We strongly encourage code deposition in a community repository (e.g. GitHub). See the Nature Research guidelines for submitting code & software for further information.

## Data

Policy information about availability of data

All manuscripts must include a data availability statement. This statement should provide the following information, where applicable:

- Accession codes, unique identifiers, or web links for publicly available datasets
- A list of figures that have associated raw data
- A description of any restrictions on data availability

The main data supporting the findings of this study are available within the paper and its Supplementary Information. The raw and analysed datasets generated during the study are too large to be publicly shared, yet they are available for research purposes from the corresponding author on reasonable request. Bacterial 16S rRNA sequencing data have been deposited in the NCBI Sequence Read Archive (accession number: PRJNA715170).

# Field-specific reporting

Please select the one below that is the best fit for your research. If you are not sure, read the appropriate sections before making your selection.

☒ Life sciences ☐ Behavioural & social sciences ☐ Ecological, evolutionary & environmental sciences

For a reference copy of the document with all sections, see nature.com/documents/nr-reporting-summary-flat.pdf

# Life sciences study design

All studies must disclose on these points even when the disclosure is negative.

| | |
|---|---|
| Sample size | Sample sizes were chosen on the basis of preliminary data from at least two pilot experiments and of previously published results. |
| Data exclusions | No data were excluded. |
| Replication | All in vitro and in vivo experiments were carried out with at least 3 biological replicates for each experimental group. |
| Randomization | Mice were assigned randomly to experimental groups. |
| Blinding | The investigators were not blinded to group allocation during the experiments and outcome assessment because our data analyses were based on objectively measurable data. |

# Reporting for specific materials, systems and methods

We require information from authors about some types of materials, experimental systems and methods used in many studies. Here, indicate whether each material, system or method listed is relevant to your study. If you are not sure if a list item applies to your research, read the appropriate section before selecting a response.

## Materials & experimental systems

| n/a | Involved in the study |
|---|---|
| ☐ | ☒ Antibodies |
| ☐ | ☒ Eukaryotic cell lines |
| ☒ | ☐ Palaeontology and archaeology |
| ☐ | ☒ Animals and other organisms |
| ☒ | ☐ Human research participants |
| ☒ | ☐ Clinical data |
| ☒ | ☐ Dual use research of concern |

## Methods

| n/a | Involved in the study |
|---|---|
| ☒ | ☐ ChIP-seq |
| ☐ | ☒ Flow cytometry |
| ☒ | ☐ MRI-based neuroimaging |

## Antibodies

Antibodies used

CD4 Monoclonal Antibody (PE, Clone: GK1.5, Cat# 12-0041-82, eBioscience)
Anti-CD45 Rat Monoclonal Antibody (APC, Clone: 30-F11, Cat# 50-162-783, BioLegend)
Anti-mouse CD45 (FITC, Clone: 30-F11, Cat# 103108, BioLegend)
Rat Anti-mouse CD8 (FITC, Clone: 53-6.7(RUO), Cat# 553035, BD Biosciences)
Anti-CD86 Rat Monoclonal Antibody (FITC, Clone: GL-1, Cat# 105006, BioLegend)
CD11c Armenian Hamster Anti-mouse (PE, Clone: N418, Cat# 50-102-20, eBioscience)
Anti-mouse PD-1 (PE-Cy7, Clone: 29F.1A12, Cat# 50-164-828, BioLegend)
Tcf1/Tcf7 Rabbit mAb (PE, Clone: C63D9, Cat# 14456S, Cell Signaling Technology)
Anti-mouse CD86 (PE-Cy7, Clone: GL1, Cat# 560582, BD Bioscience)
Anti-mouse/human CD11b (FITC, Clone: M1/70, Cat# 101206, BioLegend)
Anti-mouse F4/80 (PE, Clone: BM8, Cat# 123109, BioLegend)
Anti-mouse CD206 (APC, MMR, Clone: C068C2, Cat# 50-165-219, BioLegend)
Foxp3 Monoclonal Antibody (PE, Clone: FJK-16s, Cat# 12-5773-82, eBioscience)
CD25 Rat Anti-mouse (APC, Clone: PC61, Cat# BDB561048, BD Biosciences)
Anti-mouse IFN-γ (PE, clone: XMG1.2, Cat# 50-169-919, Biolegend)
CD44 Rat anti -Human, Mouse (FITC, Clone: IM7, Cat# 50-956-6, eBioscience)
CD62L Monoclonal Antibody (PE-Cy7, Clone: MEL 14, Cat# 50-155-28, eBioscience)
Anti-CD49b Rat Monoclonal Antibody (FITC, clone: DX5, Cat# 108905, BioLegend)
CD3 Molecular Complex Rat anti Mouse (Brilliant Violet 786, Clone: 17A2, Cat# BDB564010, BD Biosciences)
CD279 (PD-1) Rat anti-mouse (FITC, Clone: RMP1 30, Cat# 50-101-05, eBioscience)
Ly6G Monoclonal Antibody (PE, Clone: 1A8-Ly6g, Cat# 12-9668-80, eBioscience)
anti-PD-1 antibody (clone: RMP1-14, Clone: BP0146, Bioxcell)
anti-CTLA-4 antibody (clone: 9D9, Cat# BP0164, Bioxcell)
anti-CD8 (clone 2.43, Cat# BP0061, Bioxcell)

| | |
|---|---|
| | anti-CD4 (clone GK1.5, Cat# BP0003-1, Bioxcell)<br>anti-AsialoGM1 (Cat# 986-10001, Wako chemicals USA, Inc) |
| Validation | Antibody validation is indicated on the manufacture's website (cell images) and/or provided by data in the manuscript. |

## Eukaryotic cell lines

Policy information about cell lines

| | |
|---|---|
| Cell line source(s) | The CT26, MC-38 and B16F10 cell lines were obtained from the American Type Culture Collection (ATCC). The OT-I T cell line was obtained from spleen in OT-I mice. |
| Authentication | The CT26, MC-38 and B16F10 cell lines were authenticated by ATCC. |
| Mycoplasma contamination | All cell lines tested negative for mycoplasma contamination. |
| Commonly misidentified lines (See ICLAC register) | No commonly misidentified cell lines were used. |

## Animals and other organisms

Policy information about studies involving animals; ARRIVE guidelines recommended for reporting animal research

| | |
|---|---|
| Laboratory animals | For the in vivo studies, 6–8-week-old female BALB/c mice (Jackson Laboratory, or Taconic Farm, or Charles River, 18–20 g) and C57-BL/6 mice (Jackson Laboratory, 18–20 g) were used. GPR43–/– C57BL/6N male mice were provided by Prof. Chang H. Kim's lab (6–8-week-old female, 20–26 g), and 6–8-week-old CDX2-Cre NLS-APCfl/fl mice (male and female, 6–8-week-old, 19–28 g) were provided by Prof. Grace Y. Chen's lab. |
| Wild animals | The study did not involve wild animals. |
| Field-collected samples | The study did not involve samples collected from the field. |
| Ethics oversight | All work performed on animals was in accordance with, and approved by, the Institutional Animal Care & Use Committee (IACUC) at University of Michigan, Ann Arbor. |

Note that full information on the approval of the study protocol must also be provided in the manuscript.

## Flow Cytometry

### Plots

Confirm that:

☒ The axis labels state the marker and fluorochrome used (e.g. CD4-FITC).

☐ The axis scales are clearly visible. Include numbers along axes only for bottom left plot of group (a 'group' is an analysis of identical markers).

☒ All plots are contour plots with outliers or pseudocolor plots.

☒ A numerical value for number of cells or percentage (with statistics) is provided.

### Methodology

| | |
|---|---|
| Sample preparation | The sample preparation is described in Methods. |
| Instrument | BD Biosciences LSR II. |
| Software | FACSDiva was used for collection. FACSDiva and FlowJo were used for analysis. |
| Cell population abundance | Data on the abundance of the relevant cell populations are provided in the manuscript. |
| Gating strategy | Cells were gated first by morphology to exclude cell debris, doublets were then gated out by FSC-A/FSC-W, followed by exclusion of dead cells by gating on dye negative cells. |

☒ Tick this box to confirm that a figure exemplifying the gating strategy is provided in the Supplementary Information.